Morphological stability during solidification of silicon incorporating metallic impurities

Published as *Journal of Applied Physics* **115**, 163516 (2014).

Morphological Stability During Solidification of Silicon Incorporating Metallic Impurities

Jeffrey M. Warrender,[1,♦] Jay Mathews,[1,*] Daniel Recht,[2] Matthew Smith,[3] Silvija Gradečak,[3] and Michael J. Aziz[2]

[1] *U.S. Army ARDEC – Benét Laboratories, Watervliet, New York 12189, USA*

[2] *Harvard School of Engineering and Applied Sciences, Cambridge, Massachusetts 02138, USA*

[3]*Department of Materials Science and Engineering, Massachusetts Institute of Technology, Cambridge, Massachusetts 02139, USA*

ABSTRACT

We study the stability of a planar solidification front during pulsed laser melting-induced rapid solidification of silicon containing high concentrations of ion-implanted metallic impurities. We calculate the critical impurity concentration for destabilizing plane-front solidification, and introduce the "amplification coefficient", which is an empirical parameter describing the degree of amplification that must occur between the time the planar liquid-solid interface first becomes unstable, and the time of formation of morphological features of interface breakdown that are later observed in the microstructure. By connecting our calculations to experimental observations from the literature we determine this parameter for Au, Co, Cr, Fe, Ga, In, and Zn in (100) Si and Ti in (111) Si, and find that it increases with impurity diffusive speed v_D approximately as $v_D^{0.56}$. We present an approximate but simple method of estimating the maximum impurity concentration that may be incorporated in a surface layer of a given thickness without the appearance of cellular breakdown.

♦ Corresponding author. Electronic mail: jwarrend@post.harvard.edu
* Present address: University of Dayton, Dayton, OH.

I. INTRODUCTION

The use of pulsed laser melting and rapid solidification to achieve supersaturation of conventional impurities in silicon has been extensively studied.[1,2,3,4] In recent years, silicon supersaturated with sulfur has shown strong sub-band gap infrared absorption and device response.[5,6,7] This has led to interest in alternative dopants, including Au, Zn, Fe, Ti, Co, and others.[8,9,10,11] Although many of these are generally regarded as contaminants, most exhibit impurity states deep within the Si band gap, and if sufficiently high supersaturations can be achieved, such states would be expected to broaden into impurity bands, which could be one possible realization of intermediate band optoelectronic devices.[12,13,14] Recently, sub gap device response out to 2200 nm was reported in a device with a Si:Au layer.[15] One obstacle to fabricating Si layers rich in metal impurities is the susceptibility of the liquid/solid interface to morphological instability during solidification. The stability of an interface during alloy solidification[16, 17] has been treated mathematically for rapid[18] solidification, and has been studied experimentally.[19] The concentration gradient of the impurity in the liquid at the interface can cause the morphological instability and can give rise to the formation of a characteristic morphology known as “cellular breakdown”, so-called because of the cell-like appearance.[20,21,22] In a previous work[8], we reported that the depth at which breakdown was achieved was closer to the surface than the (calculated) depth at which the critical concentration for instability was exceeded, suggesting a delay between the time that a perturbation forms and the time at which it has amplified enough to exhibit morphological features that are detectable by examination of the microstructure or composition profile. We conclude that the amplification rate of the initial perturbation plays an important role in the phenomenology of breakdown.

Practical realization of layers containing high supersaturations of transition metal impurities requires knowledge about the maximum concentration that can be incorporated, and the maximum layer thickness that can be achieved without breakdown. In this work, we calculate the stability of the interface during rapid solidification for Au, In, Ga, Co, Cr, Fe, and Zn in (100) Si and Ti in (111) Si. We show that an unstable concentration in the liquid does not immediately result in breakdown of the interface, but that, by calculating the characteristic time for a perturbation to amplify, we can describe the onset of cellular breakdown in terms of an "amplification parameter". We also provide a simple method to approximate the maximum thickness that can be achieved given a desired impurity concentration, and *vice versa*.

Mullins and Sekerka[16] showed that, for a perturbation of spatial frequency ω and time-dependent amplitude $\delta(t)$ at the planar interface during solidification of a liquid, there are three contributions to the growth or suppression of the perturbation. If most of the latent heat of solidification is being removed through the solid, as it is during pulsed laser melting (PLM), the thermal gradient in the liquid or solid is always stabilizing, and is the primary stabilizing contribution at very low velocity of the liquid/solid interface. Capillarity also will always act to suppress the perturbation, and is the primary stabilizing contribution at very high interface velocity.

Working against these to destabilize the liquid-solid interface is the concentration gradient, which forms in the liquid just ahead of the interface due to partitioning of the impurity at the interface. For all impurities of interest in this work, the equilibrium concentration of impurity in the solid is lower than in the liquid. Therefore, the impurity tends to be rejected by the solid, but requires time to diffuse into the bulk of the liquid, which creates a concentration gradient in the liquid, with the highest concentration in the liquid at the interface. The higher the concentration,

the higher the impurity-induced depression of the melting point. Thus, when a bit of the solidification front jumps ahead of neighboring regions in a fluctuation, the peak advances into a liquid of higher melting point, finds itself undercooled, and accelerates. The sweeping of impurity normal to the interface along the sides of the advancing peak act to depress the melting point of the troughs in between the peaks and thereby slow their solidification. The slowing of the troughs reduces the kinetic partition coefficient, enhancing the effect. Eventually, the concentration of impurity may become so high that precipitates or liquid droplets form.[3] Because growth of the solid proceeds normally to the interface, the troughs eventually slow down so much that growth on either side of the troughs is perpendicular to the original solidification direction, and when two perpendicular solidification fronts from either side of a trough join, the characteristic cellular morphology is created.

The concentration gradient therefore acts to amplify the perturbation, and the relative magnitude of this contribution *vis à vis* the stabilizing influences of capillarity and the thermal gradient determines whether the perturbation of spatial frequency ω is amplified or decays. Mullins and Sekerka obtained a growth rate for δ,

$$\frac{\dot{\delta}}{\delta} = \frac{v\,\omega\,\{[-2\,T_M\Gamma\omega^2-(\mathcal{G}'+\mathcal{G})][\omega^*-(V/D_{liq})p]+2\,m\,G_c[\omega^*-(V/D_{liq})]\}}{(\mathcal{G}'-\mathcal{G})[\omega^*-(V/D_{liq})p]+2\,\omega m\,G_c} \quad , \qquad (1)$$

with k the partition coefficient, p=1-k, T_M the liquid melting temperature, v the interface speed, D_{liq} the diffusivity of the impurity in liquid Si, Γ the interfacial tension divided by L_M the latent heat of fusion, m the liquidus slope, $\mathcal{G}$ ($\mathcal{G}'$) the normalized thermal gradient in the liquid (solid),

$$\omega^* \equiv \left(\frac{V}{2\,D_{liq}}\right) + \left[\left(\frac{V}{2\,D_{liq}}\right)^2 + \omega^2\right]^{1/2} \qquad (2)$$

and

$$mG_c = \frac{v\,(k-1)}{D_{liq}\,k} m\, c_\infty, \tag{3}$$

with c_∞ the bulk liquid concentration. Following Mullins and Sekerka, we set $\mathcal{G}' = \mathcal{G} + vL_M/\kappa_{avg}$, with κ_{avg} the average of the liquid and solid thermal conductivities. We refer to $\dot{\delta}/\delta$ as the "amplification rate", and its inverse, τ, as the "amplification time", the time required for the perturbation amplitude to grow by a factor of *e*.

Although these equations were derived for low solidification velocity, with appropriate corrections their validity can be extended to rapid solidification as well. Aziz and Kaplan demonstrated that, at high solidification velocities, the partition coefficient *k* is increased, according to (for a dilute solution) [23,24]

$$k = \frac{k_{eq} + \frac{v}{v_D}}{1 + \frac{v}{v_D}}, \tag{4}$$

where v_D is the "diffusive speed", the ratio of the interface diffusivity of the impurity to the width of the interface, and k_{eq} the equilibrium partition coefficient. The diffusive speed has been discussed extensively in a recent paper by Recht *et al.*[8] Related to this, the kinetic liquidus slope becomes

$$m(v) = m_{eq}\left\{1 + \frac{k_{eq} - k(v)\left\{1 - \ln\left[\frac{k(v)}{k_{eq}}\right]\right\}}{1 - k_{eq}}\right\}, \tag{5}$$

with m_{eq} the equilibrium liquidus slope, which we obtain using

$m_{eq} = (1-k)R\,{T_M}^2/L_M$.[19] Together, these constitute the "Continuous Growth Model (CGM)" for partitioning during rapid solidification.[24,4]

Sekerka showed how the numerator of the right hand side of Eq. (1) can be recast as a cubic equation, whose real, positive root can be manipulated algebraically to obtain c_∞^*, the critical bulk liquid concentration.[17] Fig. 1 illustrates the relationship between c_∞, the perturbation spatial frequency ω, and the amplification rate $\dot{\delta}/\delta$. When c_∞ equals c_∞^*, the amplification rate is zero at the most unstable spatial frequency (the local maximum of the amplification rate curve). As c_∞ increases beyond c_∞^*, the most unstable spatial frequency increases, and the amplification rate becomes positive over a range of frequencies, with the amplification rate at the most unstable frequency increasing with increasing c_∞. Correspondingly, this implies that the amplification time τ decreases with increasing c_∞.

We seek to compare the results of such calculations with experimental observations of cellular breakdown for Si containing Sn[19], Ga[21], Au, Fe, Co, Cr, Zn[8], In[25], and Ti[9].

II. DATA AND ANALYSIS

A. Stability Calculation

We first used the aforementioned method of Mullins and Sekerka, with the CGM corrections, to obtain the predicted critical bulk liquid concentration c_∞^* (expressed as an atomic fraction), as a function of interface velocity for all impurities, using thermal parameters provided in Table I and impurity-specific parameters provided in Table II. The results are presented in the left column of Fig. 2. Additionally, using equation (1), and the definition of τ as the inverse of $\dot{\delta}/\delta$, we calculated the amplification time τ as a function of the ratio c_∞/c_∞^* for two representative interface velocities, v=1 m/s and v=10 m/s, and the resulting values are presented in the center

and right columns of Fig. 2, respectively. The diffusive speed v_D is generally obtained by performing a 1D diffusion calculation[26] and adjusting v_D until good agreement between the predicted impurity depth profile and an experimental depth profile obtained from Secondary Ion Mass Spectrometry (SIMS) or Rutherford Backscattering Spectrometry (RBS) is achieved. Uncertainty arising from the calibration of the depth and concentration axes in the depth profiles creates uncertainty in the calculated v_D, and a possible error of up to a factor of 2 can be assumed. Therefore, for each impurity, we calculated c_∞^* and τ for the literature value of v_D,[25] and also for a value a factor of 2 higher and lower. Results for all three values are presented for each impurity.

The left column presents the neutral stability condition for each impurity; growth under conditions (interface speed and bulk liquid concentration) that fall below the curve are stable, and above the curve, unstable. The plots in this column therefore identify the conditions under which stable growth can be expected. The center and right columns are calculated for the most unstable spatial frequency ω corresponding to the interface speed v for that column.

Although the middle and right columns of Fig. 2 show that amplification times are shorter for v=10 m/s compared to 1 m/s, it must be remembered that the abscissa of these columns is *normalized* bulk liquid concentration, and the stable bulk liquid concentration will be greater at higher speed; thus, these columns show the effect of *excess* concentration on the amplification time.

B. Cellular Breakdown

Next, we seek to connect these calculations with the experimentally observed onset of cellular breakdown in layers containing these impurities. Breakdown manifests in two ways – visually,

the cell walls are observable in plan view using the backscatter detector in a scanning electron microscope (SEM) or in cross section using a Transmission Electron Microscope (TEM); and, compositionally, the onset of breakdown is indicated by an abrupt increase in impurity concentration with decreasing depth in the solid, resulting from excess impurity being trapped in cell walls. Hoglund noted that the latter effect can be detected deeper in the layer can than the former effect.[19] We use literature results, which were obtained using microscopy for Ga and composition for all other impurities, to set an experimental "breakdown depth" d_B for each impurity. The ion implantation and laser melting parameters that were used to fabricate these samples are provided in Table III, as are the literature values of d_B.

Using experimental depth profiles (when available) or SRIM calculations (when not) for the initial concentration depth profile,[27] and the results of experimentally validated 1D heat flow calculations[19] to estimate the thermal conditions that each sample experienced, we use a numerical solution of the 1D diffusion equation with partitioning at a moving boundary [26] to predict the concentration depth profile that each sample would have experienced under the conditions given in Table III. We seek the time required for amplification of a perturbation that forms when the interface is at any given depth *d*. To make this calculation tractable, we make several simplifying assumptions. (i) The spatial frequency of the perturbation that forms at *d* is unique, and is the most unstable frequency at that depth. (ii) The growth of this perturbation, having spatial frequency $\omega(d)$, is unaffected by the growth of other perturbations and their associated spatial frequencies. (iii) The perturbation grows at a constant rate, given by $\dot{\delta}/\delta$, which, according to equation (1), is a function of $\omega(d)$, of $v(d)$, the interface speed at *d*, and of the ratio c_∞/c_∞^* at *d*. The growth can therefore be described by a characteristic time for amplification by a factor of *e*, τ, which is the inverse of $\dot{\delta}/\delta$. (iv) By the time the perturbation

has amplified by a factor of e, the interface will have traveled toward the surface by a distance $\ell = v(d)\ \tau$. (v) To obtain c_∞/c_∞^*, c_∞ can be approximated by a time-independent curve, and (vi) $c_\infty(d)$ can be obtained from that curve by adding a constant, impurity-specific (negative) offset to d, which approximately corresponds to the spatial extent of the tail of the interface concentration gradient extending into the liquid (essentially, it is the "distance" from the interface to the bulk liquid). With these assumptions, we obtain a unique value of τ for each d. Fig. 3(a) illustrates the method, using representative data from a calculation of In in Si under the conditions given in Table II.

Assumptions (v) and (vi) are made for computational convenience, but are justified by examination of Fig. 3(c), which shows the concentration depth profile of In in Si for several different time steps during solidification. The liquid concentration beyond the tail of the concentration peak is approximately uniform for all time steps, and is slowly-varying; therefore, assuming a constant offset value, while technically inaccurate,[28] only contributes a small possible error, which we estimate below. Assumption (iii), and its derivative assumption, (iv), are not realized in the actual solidification, because the amplification rate at a fixed frequency increases as the ratio c_∞/c_∞^* increases; and additionally, the speed changes with depth. However, if we allow assumption (i) to hold, we find that the amplification rate quickly converges to a maximum of a factor of between 1.4-2.2 of its initial value (impurity-dependent) as c_∞/c_∞^* is increased, assuming constant speed; if the decreasing speed is taken into account in the calculated amplification rate, this factor is even smaller. And, the speed decreases by less than 20% between the depth at which c_∞^* is achieved in the liquid and the depth at which a perturbation is observed. Therefore, treating v and τ as constant are reasonable approximations that have the advantage of making the subsequent calculations tractable. Finally, we acknowledge that in the

actual solidification, all wavelengths are present simultaneously, and that assumption (ii) is only strictly true when the amplitudes remain small.

C. Amplification Coefficient

Using the approach described above, we can calculate a curve for τ as a function of depth, and can use it to calculate a predicted breakdown depth *vs. d*. Here we face the complication that we do not know *a priori* how many periods of amplification will be required for breakdown to be achieved. We introduce a quantity ξ as an empirical parameter, which we refer to as the "amplification coefficient". For a perturbation that first amplifies when the interface is at depth *d*, the depth at which breakdown would be expected occur is $d - v\xi\tau$, where v and τ depend on *d*. We plot the results of this calculation in Fig. 4 for the case of In. The solid line corresponds to c_∞, and sets the value of *d* for the plot of the expected breakdown depth curve. The abscissa of the breakdown depth curve is $d - v\xi\tau$, and the ordinate is the bulk liquid concentration c_∞ at the time that the interface was at depth *d*. In other words, the horizontal distance between the breakdown depth curve and the bulk liquid concentration curve, for a given concentration, is the "breakdown length", $v\xi\tau$, which is the distance the interface will have traveled before sufficient amplification has occurred for breakdown. The predicted breakdown depth, then, will be the right-most (i.e., deepest) point on the breakdown depth curve, and this can be compared to the observed thickness of the broken-down layer.

Fig. 4 has several features of note. First, as mentioned in a previous paper[8], the experimental breakdown depth does not occur at the crossing of c_∞ and c_∞^*, validating the intuition that the perturbation would need to amplify before breakdown is observable. Second, because we assumed a constant value for v and τ, , we can vary ξ until we achieve agreement between the

breakdown curve and the experimental breakdown depth. For In diffusion simulated using the conditions of Table II, we find that ξ=7.8 gives agreement with the experimental breakdown depth d_B of 106 nm.

Before we can fully generalize this method for all impurities, we first consider a single impurity at several implantation doses, to ascertain whether ξ has a dose dependence. In Ref. 9, we reported on the behavior of Ti in Si (111) at various implantation doses. Identical substrate, implantation energy, and laser melting conditions were used for all doses, making this system ideal for this comparison. In this work, we considered four implantation doses: 1×10^{16} at./cm^2, 3×10^{15} at./cm^2, 8×10^{14} at./cm^2, and 1×10^{14} at./cm^2. As reported in Table III, all except 1×10^{14} at./cm^2 showed a broadened surface concentration peak in SIMS depth profiles, which is known to be characteristic of cellular breakdown.[19, 21] We used SIMS as-implanted profiles for the initial depth profile, and generated a melt depth *vs.* time curve using the intensity profile of the Nd:YAG laser. Using these, we generated a c_∞^* and c_∞ curve for each dose, using the best-fit value of v_D obtained from fitting the post-melting SIMS profile for that dose. Finally, setting ξ to 4.06, we calculated the breakdown depth curve $d - v\,\xi\tau$ for each dose, using $c_\infty(d)$ for that dose as the ordinate. Fig. 5 shows the resulting curves, along with vertical lines corresponding to the breakdown depths observed in SIMS data. The agreement between the rightmost point of each breakdown depth curve and the observed experimental breakdown depth for that same dose is excellent. (Note particularly that the lowest dose, 1×10^{14} at./cm^2 , did not show breakdown experimentally, and in Fig. 5, its breakdown depth curve has a negative abscissa for all concentrations, indicating that, for all $c_\infty(d)$, $v\xi\tau > d$, and therefore, the layer would not have been expected to show breakdown.) We conclude that there is no value to be added to the model by including a dose-dependence to ξ.

We followed a similar method to obtain the amplification coefficient for all of the impurities previously mentioned, and present the results in Table IV. These may be used in the simple method described in the next section to estimate the critical thickness for breakdown for these impurities.

We identify two potential sources of error in ξ. First, we estimate the error in the offset from *d* as at most 20%, which results in an error in ξ of about 6%. Second, using Fig. 2, at 1 m/s, an error in v_D of a factor of 2 could result in an error in τ on the order of 20% (for Au), which could result in an adjustment to ξ of 16%. Adding these two estimates together in quadrature, we estimate a maximum total error of 17% in our calculated values of ξ.

We can corroborate our observation by comparing the most unstable wavelength ($\lambda = 2\pi/\omega$) at $d = d_B + v\xi\tau$, the depth at which the "breakdown perturbation" formed, to the average cell wall spacing observed in *post mortem* microscopy of the broken-down layer. Narayan reports experimental cell wall spacings of 50 nm and 70 nm for In and Ga, respectively, under comparable conditions to those of our calculations.[21] For In, under our model, the breakdown perturbation first amplified when the interface was at a depth of 180 nm, and λ = 28 nm; for Ga, the corresponding values are 120 nm and 57 nm, respectively. These results are in reasonably good agreement with the experimental observations. Exact agreement of the periodicity would have resulted had the breakdown perturbations first amplified at 230 nm (In) and 150 nm (Ga), in the model.

D. Predicting the Critical Thickness

A practical question confronting the experimentalist or the technologist pertains to the maximum thickness that can be achieved for a given concentration of a particular impurity before the

observation of breakdown, or the maximum concentration that can be achieved for a given thickness. We now provide a simple method for estimating this. We first acknowledge that direct experimental observation of the bulk liquid concentration is impractical. We use 1D diffusion simulations to estimate a quantity ζ, with $\zeta \equiv c_\infty^{max}/c_s^{max}$, with c_s^{max} the maximum solid concentration after solidification is complete, disregarding the concentration peak near the surface that results from the "snowplowing" of impurity to the surface during partitioning. Fig. 7 shows, graphically, our method for obtaining c_∞^{max} and c_s^{max}. We present the values of ζ for each impurity in Table IV. Unlike ξ, ζ may have a weak dose dependence; our values for Ti changed by slightly less than a factor of 2 between the 1×10^{16} at./cm^2 dose and the 8×10^{14} at./cm^2 dose. But as a tool for approximating, we believe ζ is nevertheless useful.

Assuming one has a target concentration c_s and the ability to achieve a (fixed) interface velocity *v*, the following method is used to obtain the critical thickness of a layer that does not exhibit breakdown. First, Fig. 2 is used to obtain the critical bulk liquid concentration c_∞^*. Next, c_s is multiplied by ζ (from Table IV) to provide a target bulk liquid concentration c_∞. Assuming for simplicity that *v* is either 1 m/s (excimer) or 10 m/s (Nd:YAG), the appropriate column of Fig. 2 is then used to obtain τ at c_∞/c_∞^*. Using ξ from Table IV, the critical thickness is simply

$$d_{crit} = v\xi\tau. \tag{6}$$

To obtain the maximum achievable concentration for a given layer thickness, the reverse process is used.

As a simple example, we consider the case of a layer implanted with Au and irradiated with an Nd:YAG laser, which provides an interface velocity of 6 m/s. As an approximation, we round this up to 10 m/s so as to be able to use the data in Fig. 2. The critical bulk liquid concentration

c_∞^* is 3.6×10^{-4} (atomic fraction). Supposing we seek a layer concentration of 5×10^{20} at./cm^3, we use the atomic density of solid Si (5×10^{22} at./cm^3) and the value of ζ for Au, 12, to calculate c_∞=0.12, and c_∞/c_∞^*=333; using the 10 m/s graph in Fig. 2, we obtain τ=0.063 ns. Thus, our maximum layer thickness, using equation (6), is $d_{crit} = 9.1$ nm. (Had we performed the calculation using data for 6 m/s, the result would have been 8.2 nm). If we switch substrates, to Si (111), for which v_D <200 m/s, then τ becomes 0.09 ns, and d_{crit} = 13 nm.

For an approximate experimental validation, we consider the case of Fig. 2 in Ref. 8, for a Si:Au layer irradiated with an excimer laser (v=3m/s), for which the critical bulk liquid concentration c_∞^* is 2.0×10^{-5} (atomic fraction). Assuming a desired concentration of 2×10^{19} at./cm^3, c_∞/c_∞^*=240, and τ is approximately 2.0 ns, giving an estimated maximum layer thickness $d_{crit} = 86$ nm. The sample in Ref. 8 exhibits a solid concentration of 2×10^{19} at./cm^3 at a depth of about 220 nm, and the depth at which breakdown is observed, d_B, is about 150 nm, for a distance of 70 nm, in reasonable agreement with our approximate calculation.

E. Relationship between ξ and v_D

Finally, we ask whether any systematic dependence of ξ across impurities is observed. In Fig. 7, we plot ξ as a function of v_D for those impurity layers fabricated in (100) material. (We exclude Ti from this plot because its calculated v_D would likely be different were it implanted into (100) material [26], and c_∞^* , τ, and ξ would therefore be different as well). Per section II.C above, error bars corresponding to 17% of ξ, along with horizontal error bars of a factor of +/- 2, are included in Fig. 7.

If the Sn data point from Ref. 19 is excluded, we observe a strong correlation between ξ and v_D for those layers that were grown in (100) Si. A fit with a power law dependence $\xi \sim {v_D}^{0.56}$ gives an R^2 value of 0.96. A weak correlation between ξ and D_{liq} or k_{eq} may be present as well. We are uncertain why the Sn data point from Ref. 19 does not fall on the curve, but we note that we were unable to reproduce their empirical melt depth of 320 nm in 1D heat flow calculations using all of the sample and laser parameters that they provided; we instead calculate a melt depth of 180 nm. A deeper melt would result in a slower interface, which would lower c_∞^* and, correspondingly, would lower τ; therefore, a higher value of ξ would have resulted.

III. SUMMARY

In summary, we calculated the critical bulk liquid concentration for interface stability during solidification of laser-melted (100) silicon containing Au, Co, Cr, Fe, Ga, In, or Zn, and for (111) silicon containing Ti. We found that the interface does not break down immediately upon achievement of a bulk liquid concentration in excess of the critical concentration, but that instead, a perturbation that forms at some depth d will require an impurity-dependent length for amplification, given by $v\xi\tau$, where v and τ are the interface speed and inverse amplification rate at depth d, respectively, and ξ is the empirical "amplification coefficient". We found that ξ has a statistically significant power law dependence on the diffusive speed v_D, with a power of 0.56. We also observed a tentative correlation between ξ and the ratio of the maximum bulk liquid concentration to the maximum solid concentration after solidification. More substantial theoretical work will be required in order to explain the dependence of ξ on v_D. A simple method for estimating the maximum concentration or layer thickness that can be achieved for a given impurity and interface speed was provided.

REFERENCES

1. C.W. White, S.R. Wilson, B.R. Appleton, and F.W. Young, *Journal of Applied Physics* **51**, 738 (1980).
2. M. Finetti, P. Negrini, S. Solmi, and D. Nobili, *Journal of the Electrochemical Society* **128**, 1313 (1981).
3. C.W. White, *Journal de Physique* **44**, C5-145 (1983).
4. J.A. Kittl, P.G. Sanders, M.J. Aziz, D.P. Brunco, and M.O. Thompson, *Acta materialia* **48**, 4797 (2000).
5. T.G. Kim, J.M. Warrender, and M.J. Aziz, *Applied Physics Letters* **88**, 241902 (2006).
6. B.P. Bob, A. Kohno, S. Charnvanichborikarn, J.M. Warrender, I. Umezu, M. Tabbal, J.S. Williams, and M.J. Aziz, *Journal of Applied Physics* **107**, 123506 (2010).
7. A.J. Said, D. Recht, J.T. Sullivan, J.M. Warrender, T. Buonassisi, P.D. Persans, and M.J. Aziz, *Applied Physics Letters* **99**, 073503 (2011).
8. D. Recht, M.J. Smith, S. Charnvanichborikarn, J.T. Sullivan, M.T. Winkler, J. Mathews, J.M. Warrender, T. Buonassisi, J.S. Williams, S. Gradečak, and M.J. Aziz, *Journal of Applied Physics* **114**, 124903 (2013).
9. J. Mathews, A.J. Akey, D. Recht, G. Malladi, H. Efstathiadis, M.J. Aziz, and J.M. Warrender, *Applied Physics Letters, in press.*
10. J. Olea, M. Toledano-Luque, D. Pastor, E. San-Andrés, I. Mártil, and G. González-Díaz, *Journal of Applied Physics* **107**, 103524 (2010).
11. Y. Zhou, F. Liu, and X. Song, *Journal of Applied Physics* **113**, 103702 (2013).
12. A. Luque and A. Martí, *Physical Review Letters* **78**, 5014 (1997).

13. J.J. Krich, B.I. Halperin, and A. Aspuru-Guzik, *Journal of Applied Physics* **112**, 013707 (2012).

14. J.T. Sullivan, C.B. Simmons, J.J. Krich, A.J. Akey, D. Recht, M.J. Aziz and T. Buonassisi, *Journal of Applied Physics* **114**, 103701 (2013).

15. J.P. Mailoa, A.J. Akey, C.B. Simmons, D. Hutchinson, J. Mathews, J.T. Sullivan, D. Recht, M.T. Winkler, J.S. Williams, J.M. Warrender, P.D. Persans, M.J. Aziz, and T. Buonassisi, *Nature Communications* 5, 3011 (2014)

16. W.W. Mullins and R.F. Sekerka, *Journal of Applied Physics* **35**, 444 (1964)

17. R.F. Sekerka, *Journal of Applied Physics* **36**, 264 (1965).

18. J.W. Cahn, S.R. Coriell, and W.J. Boettinger, in *Laser and Electron Beam Processing of Materials*, edited by C.W. White and P.S. Peercy, (Academic Press, New York, 1980), p.89.

19. D.E. Hoglund, M.O. Thompson, and M.J. Aziz, *Physical Review B* **58**, 189 (1998).

20. A.G. Cullis, D.T.J. Hurle, H.C. Webber, N.G. Chew, J.M Poate, P. Baeri, and G. Foti, *Applied Physics Letters* **38**, 642 (1981).

21. J. Narayan, *Journal of Applied Physics* **52**, 1289 (1981).

22. J. Narayan, *Journal of Crystal Growth* **59**, 583 (1982).

23. We performed simulations in which the non-dilute form of *k* was used, but found little difference between the retained impurity concentrations for the two cases.

24. M.J. Aziz and T. Kaplan, *Acta metallurgica* **36**, 2335 (1988).

25. Data and best fit v_D for In from D. Recht and M.J. Aziz, unpublished.

26. R. Reitano, P.M. Smith, and M.J. Aziz, *Journal of Applied Physics* **76**, 1518 (1994).

27. www.srim.org

28. The decay length of the spike in reality equals D_{liq}/v in the quasistationary approximation.

$\mathcal{G}$	Thermal gradient in liquid	2×10^4 K/m
T_M	Melting temperature of Si	1685 K
L_M	Latent heat of fusion at melting temperature	4.19×10^9 J/m^3
γ (= ΓL_M)	Interfacial tension	0.36 J/m^2

Table I. Parameters used in calculations of c_∞^{max}. All values from Ref. 19.

Impurity	v_D (m/s)	D_{liq} (cm^2/s)	k_{eq}	Offset (nm)
Au [8] (*)	350	6×10^{-5}	0.000025	30
Co [8]	10 000	1.8×10^{-5}	0.00001	5
Cr [8]	10 000	1	0.000011	5
Fe [8]	100	3.2×10^{-5}	0.000007	10
Ga [21]	35	3.6×10^{-4}	0.008	30
In [26](*)	100	1.6×10^{-4}	0.0004	25
Sn [19]	17	2.5×10^{-4}	0.016	
Ti [9]	20 000	6×10^{-4}	0.000002	20
Zn [8]	1 000	3.2×10^{-4}	0.00001	30

Table II. Parameters used in calculation of thermal properties and in diffusion calculations. (*) For Au and In, the literature values reported in Table II were used to generate Fig. 2 (note that the literature value for v_D for In is 85.5 m/s[26]); for all other calculations, the best-fit values from 1D diffusion simulations in comparison with SIMS measurements were used, namely, D_{liq} = 3×10^{-4} cm^2/s (both), and v_D=400 m/s (Au) and 200 m/s (In).

Impurity	Orientation	Ion energy (keV)	Implantation dose (at/cm^2)	Laser	Laser fluence (J/cm^2)	d_B (nm)
Au [8]	(100)	325	1×10^{16}	XeCl	2.0	150
Co [8]	(100)	120	1×10^{16}	XeCl	2.0	150
Cr [8]	(100)	95	5×10^{15}	XeCl	2.0	110
Fe [8]	(100)	140	1×10^{16}	XeCl	2.0	140
Ga [21]	(100)	100	1.2×10^{16}	Ruby (*)	1.5	50
In [25]	(100)	160	1×10^{16}	XeCl	2.0	106
Sn [19]	(100)	120	3.5×10^{15}	XeCl	1.25	70
Ti [9]	(111)	15	1×10^{16}, 3×10^{15}, 8×10^{14}, 1×10^{14}	Nd:YAG	0.75	70, 50, 25, N/A
Zn [8]	(100)	120	5×10^{15}	XeCl	2.0	43

Table III. Experimental parameters for impurity implantation, laser melting, and observed breakdown depth d_B. For lasers, pulse intensity profiles were obtained from the actual lasers used, with the exception of (*) Ruby, for which a Gaussian pulse with FWHM 15 ns was used.

Impurity	ξ	ζ
Au	14.4	12
Co	82.6	23
Cr	107.9	16
Fe	7.4	1.3
Ga	3.6	1.6
In	7.8	5.6
Ti	4.06	450 (1×10^{16} at./cm^2) 660 (3×10^{15} at./cm^2) 720 (8×10^{14} at./cm^2)
Zn	28.8	20

Table IV. Best values of ξ and ζ for each impurity.

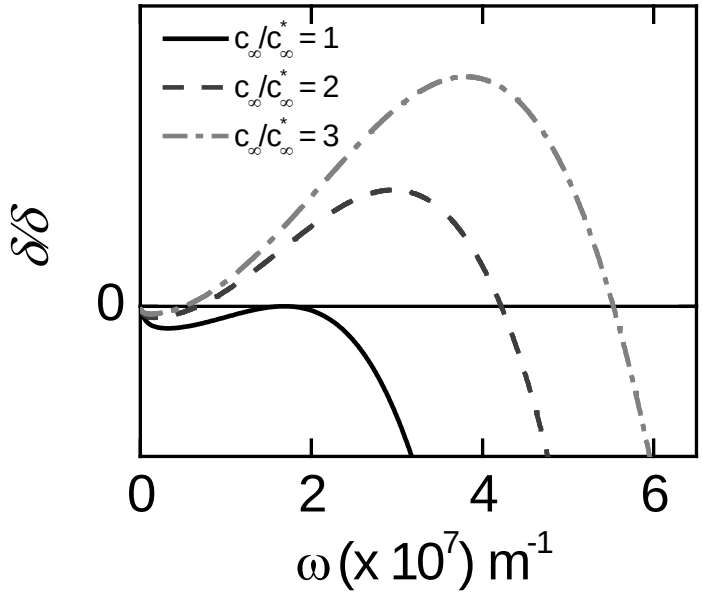

Fig. 1. Amplification rate *vs*. perturbation spatial frequency ω at bulk liquid concentrations 1 (solid), 2 (dash), and 3 (dash-dot) times the critical bulk liquid concentration. As the bulk liquid concentration exceeds the critical concentration, the amplification rate becomes positive, and a perturbation will grow. The most unstable wavelength becomes shorter with increasing excess concentration.

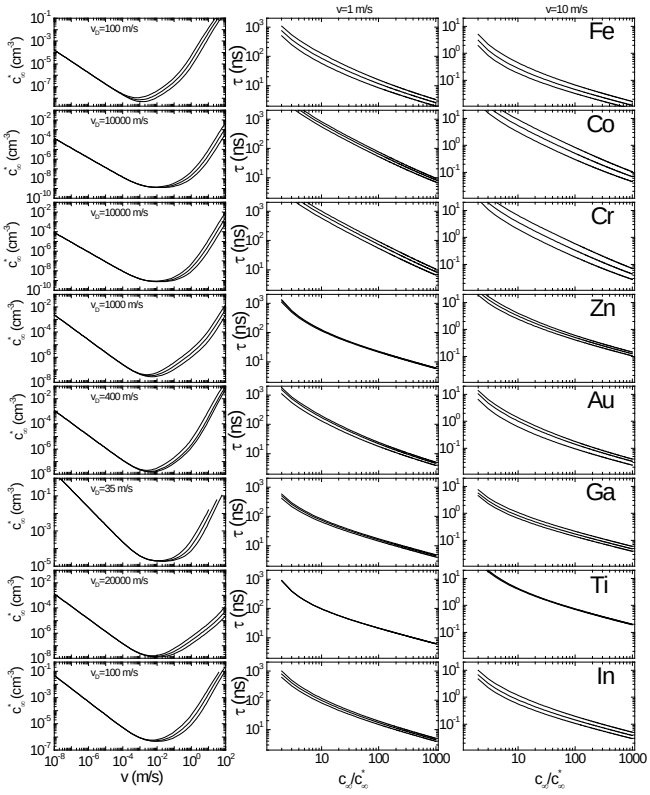

Fig. 2. Neutral stability curves (left column) for various impurities in Si (100). (exception: Ti was obtained for Si (111).) The amplification time, τ, as a function of ratio c_∞/c_∞^*, at an interface speed of 1 m/s (center column) and 10 m/s (right column). All data were computed for three multiples of the best fit value for v_D, namely: $v_D/2$, v_D, and 2 v_D. In the left column, these three values resulted in the lower, middle, and upper curves, respectively. In the center and right columns, they produced the upper, middle, and lower curves, respectively.

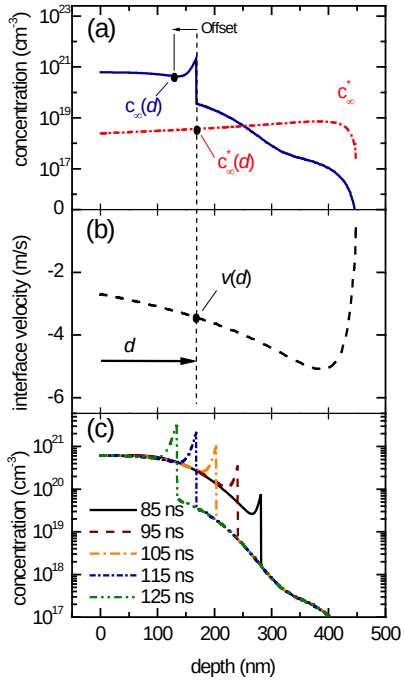

Fig. 3. (color online) Schematic illustration of the method for obtaining τ when the liquid-solid interface is at depth *d*. (a) and (b) The interface velocity *v*(*d*) (dashed line) is obtained from 1D heat flow calculations, and the critical bulk liquid concentration (dash-dot line) is calculated using the interface speed as an input. The impurity concentration as a function of depth (solid blue line) is obtained from a 1D diffusion calculation, and c_∞ is taken to be the impurity concentration in the liquid at a negative offset from the interface depth *d*, to avoid the tail that results from partitioning of the impurity at the interface. (c) Concentration depth profiles at various time steps under identical conditions to (a). For any time step, the bulk liquid concentration at depths shallower than the tail of the interface concentration maxima approximately falls onto the same curve; we use this curve as $c_\infty(d)$.

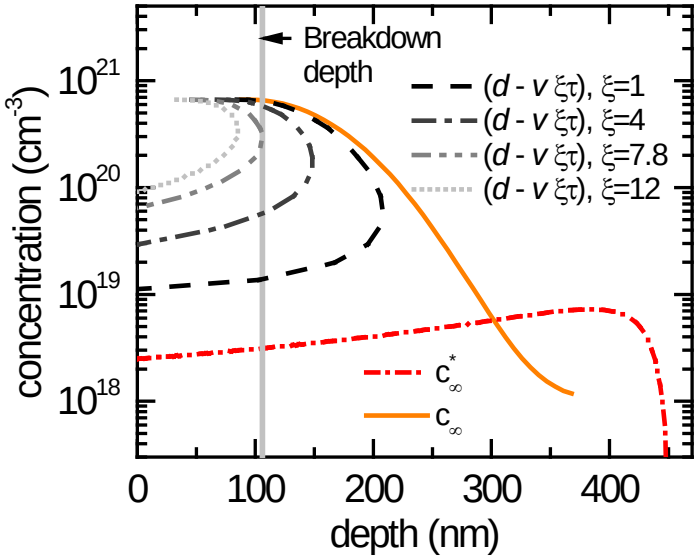

Fig. 4. (color online) Illustration of the method for obtaining the amplification coefficient ξ, for the case of In implanted at 200 keV to a dose of 1×10^{16} at./cm^2, and melted by a XeCl excimer laser at a fluence of 2 J/cm^2. The critical bulk liquid concentration (short dash-dot line) is calculated using the interface velocity v *vs.* depth d obtained from 1D heat flow calculations, and the bulk liquid concentration (solid line) is obtained from 1D diffusion calculations. The predicted breakdown depth is plotted for varying values of ξ. The ordinate value of these curves corresponds to the bulk liquid concentration when the interface is at depth d, and the abscissa, $d - v\,\xi\tau$, is the predicted breakdown depth for a perturbation that begins at that depth d. Therefore, the rightmost value of the curve is the predicted breakdown depth for the layer. For In, the experimentally observed breakdown depth (vertical solid line) is 106 nm. Setting $\xi = 7.8$, the abscissa of the rightmost point on the breakdown depth curve is equal to the breakdown depth.

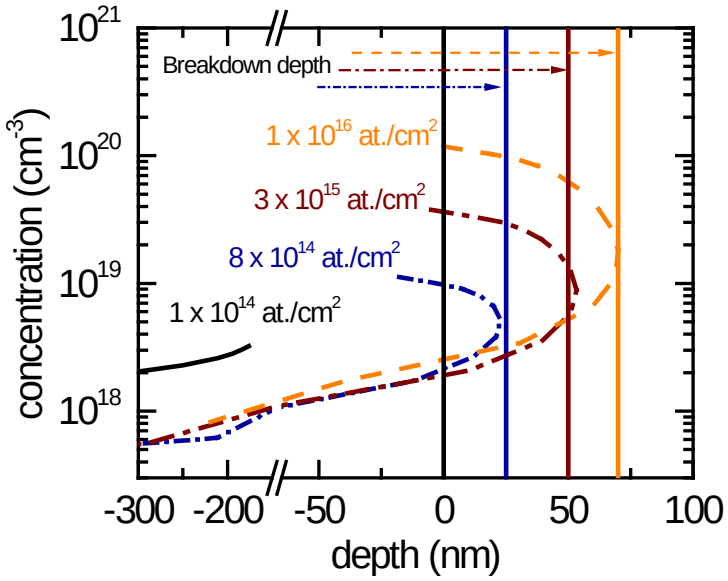

Fig. 5. (color online) Predicted breakdown depth $d - v\,\xi\tau$ for several implant doses of Ti in (111) Si, for pulsed laser melting with an Nd:YAG laser at 0.75 J/cm^2. The same value of ξ (4.06) is used for all doses. Vertical lines show the experimentally observed breakdown depths. The agreement between the rightmost point of each of the breakdown depth curves, and the corresponding experimental breakdown depth, is excellent. For the 1×10^{14} at./cm^2 dose sample, the breakdown depth curve never reaches a positive depth, indicating that breakdown is not expected. This agrees with the experimental observation.

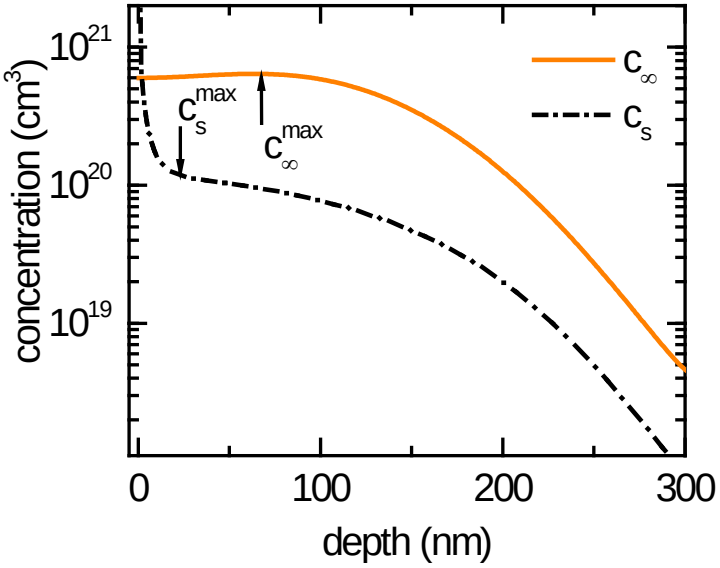

Fig. 6.(color online) Comparison of bulk liquid concentration at 45 ns (solid line) and solid concentration after solidification (dash-dot line) for In. The arrows denotes the peak of the bulk liquid concentration and solid concentration, which are used for calculation of the ratio $\zeta = c_\infty/c_s$.

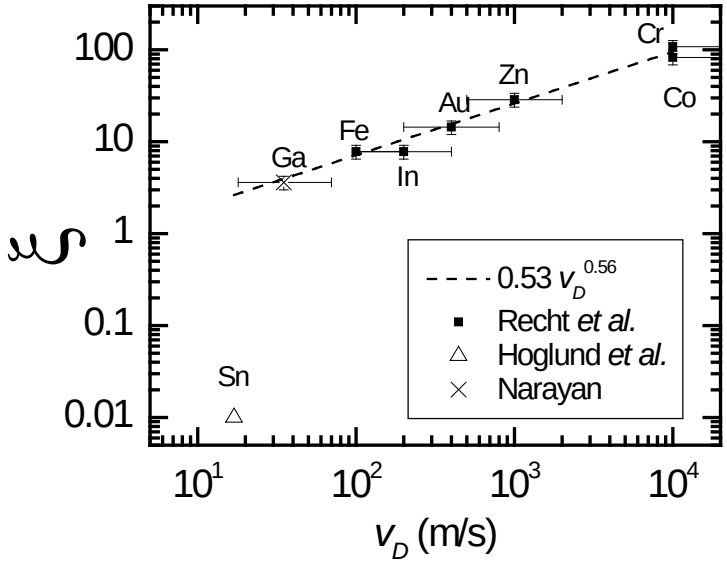

Fig. 7. Amplification coefficient ξ as a function of v_D. With the exception of the Sn point from Ref. 19, the ξ *vs.* v_D data show power law behavior. The error bars show a possible factor of 2 error in v_D and a possible error of 17% in ξ. (Note: fits to v_D from Ref. 8 are lower bounds for Fe, Co, and Cr).